Journal of The Electrochemical Society

The Electrochemical Society
Advancing solid state & electrochemical science & technology

OPEN ACCESS

Degradation of Commercial Lithium-Ion Cells as a Function of Chemistry and Cycling Conditions

To cite this article: Yuliya Preger *et al* 2020 *J. Electrochem. Soc.* **167** 120532

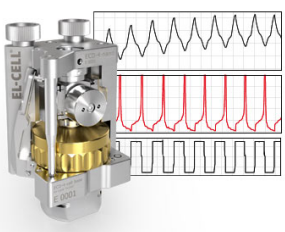
View the article online for updates and enhancements.

You may also like

- Study of Novel Nonflammable Electrolytes in Sandia-Built Li-Ion Cells
Ganesan Nagasubramanian and Christopher J. Orendorff
- Investigating the Role of Energy Density in Thermal Runaway of Lithium-Ion Batteries with Accelerating Rate Calorimetry
Joshua Lamb, Loraine Torres-Castro, John C. Hewson et al.
- Direct numerical simulation of mechanical response in synthetic additively manufactured microstructures
Theron M Rodgers, Joseph E Bishop and Jonathan D Madison

Measure the Electrode Expansion in the Nanometer Range.
Discover the new ECD-4-nano!

EL-CELL® electrochemical test equipment



- Battery Test Cell for Dilatometric Analysis (Expansion of Electrodes)
- Capacitive Displacement Sensor (Range 250 µm, Resolution ≤ 5 nm)
- Detect Thickness Changes of the Individual Electrode or the Full Cell.

www.el-cell.com +49 40 79012-734 sales@el-cell.com

This content was downloaded from IP address 193.119.84.192 on 02/02/2024 at 07:12

Journal of The Electrochemical Society, 2020 **167** 120532

Degradation of Commercial Lithium-Ion Cells as a Function of Chemistry and Cycling Conditions

Yuliya Preger,[1,*,z] Heather M. Barkholtz,[1] Armando Fresquez,[2] Daniel L. Campbell,[3] Benjamin W. Juba,[4] Jessica Romàn-Kustas,[4] Summer R. Ferreira,[5] and Babu Chalamala[1,*]

[1]*Energy Storage Technology and Systems, Sandia National Laboratories, Albuquerque, New Mexico, United States of America*
[2]*Advanced Power Sources R&D, Sandia National Laboratories, Albuquerque, New Mexico, United States of America*
[3]*Statistical Sciences, Sandia National Laboratories, Albuquerque, New Mexico, United States of America*
[4]*Materials Reliability, Sandia National Laboratories, Albuquerque, New Mexico, United States of America*
[5]*Renewable and Distributed Systems Integration, Sandia National Laboratories, Albuquerque, New Mexico, United States of America*

Energy storage systems with Li-ion batteries are increasingly deployed to maintain a robust and resilient grid and facilitate the integration of renewable energy resources. However, appropriate selection of cells for different applications is difficult due to limited public data comparing the most commonly used off-the-shelf Li-ion chemistries under the same operating conditions. This article details a multi-year cycling study of commercial $LiFePO_4$ (LFP), $LiNi_xCo_yAl_{1-x-y}O_2$ (NCA), and $LiNi_xMn_yCo_{1-x-y}O_2$ (NMC) cells, varying the discharge rate, depth of discharge (DOD), and environment temperature. The capacity and discharge energy retention, as well as the round-trip efficiency, were compared. Even when operated within manufacturer specifications, the range of cycling conditions had a profound effect on cell degradation, with time to reach 80% capacity varying by thousands of hours and cycle counts among cells of each chemistry. The degradation of cells in this study was compared to that of similar cells in previous studies to identify universal trends and to provide a standard deviation for performance. All cycling files have been made publicly available at batteryarchive.org, a recently developed repository for visualization and comparison of battery data, to facilitate future experimental and modeling efforts.
© 2020 The Author(s). Published on behalf of The Electrochemical Society by IOP Publishing Limited. This is an open access article distributed under the terms of the Creative Commons Attribution Non-Commercial No Derivatives 4.0 License (CC BY-NC-ND, http://creativecommons.org/licenses/by-nc-nd/4.0/), which permits non-commercial reuse, distribution, and reproduction in any medium, provided the original work is not changed in any way and is properly cited. For permission for commercial reuse, please email: permissions@ioppublishing.org. [DOI: 10.1149/1945-7111/abae37]

Manuscript submitted May 27, 2020; revised manuscript received July 30, 2020. Published September 2, 2020. *This was paper 605 presented at the Dallas, Texas, Meeting of the Society, May 26–May 30, 2019.*

Supplementary material for this article is available online

Energy storage systems (ESS) consisting of Li-ion batteries are expected to play a critical role in the integration of intermittent renewable energy resources into the electric grid, as well as to provide back-up power and enhanced resiliency.[1–3] For applications in the electric grid, ESS are expected to last for a decade or even longer. A typical MWh system may contain as many as 100,000 cells assembled into packs. To ensure system safety and reliability, cells must be selected based on application specific requirements and performance characteristics. Yet there are few comparisons of popular commercial cells under similar operating conditions. In this work, we detail the cycling performance of commercial LFP ($LiFePO_4$), NCA ($LiNi_xCo_yAl_{1-x-y}O_2$), and NMC ($LiNi_xMn_yCo_{1-x-y}O_2$) cells with an 18650 form factor, in the broadest such comparison to be reported in a peer-reviewed publication.

Battery specification sheets from manufacturers primarily focus on safety metrics, such as current, voltage, and temperature bounds, with limited information on performance metrics. Many publications in the open literature have examined the long-term performance and aging of commercial Li-ion cells in order to fill this gap. There are notable recent studies for each of the chemistries—LFP,[4–11] NCA,[6,10,12–14] and NMC,[6,15–17]—under calendar, constant current square wave cycle, and grid duty cycle aging. However, each of these studies typically focuses on a single chemistry under a limited subset of conditions to understand the influence of a particular variable, such as temperature, or the emergence of a particular degradation phenomena, such as Li plating.

The short-term cycling performance[18] and calorimetry[19] for the cells selected for the present study has been reported previously, and this work is part of a broader effort at Sandia National Laboratories to characterize the safety and reliability of commercial Li-ion cells. This study examines the influence of temperature, depth of discharge (DOD), and discharge current on the long-term degradation of the commercial cells. Cycling was carried out under constant current square wave duty cycles rather than grid duty cycles to better understand the contribution of specific and simple cycling conditions to the degradation process. Various metrics for comparing cell degradation were investigated, including equivalent full cycle count, discharge energy, and round-trip efficiency. The degradation of the cells in this study was compared to that of similar cells in previous studies to provide a standard deviation for performance and facilitate a more data-informed adoption of these batteries.

Experimental Conditions

Tested batteries.—The commercial 18650 cells examined in this work were manufactured by the following companies: LFP from A123 Systems (Part #APR18650M1A, 1.1 Ah), NCA from Panasonic (Part #NCR18650B, 3.2 Ah), and NMC from LG Chem (Part #18650HG2, 3 Ah). The three batteries were selected because they included common electrode formulations and were manufactured by reputable companies. Table I provides additional specifications for each cell, including the manufacturer-recommended operating bounds. According to inductively coupled plasma optical emission spectrometry (ICP-OES), the elemental composition of the NMC cathode is $Ni_{0.84}Mn_{0.06}Co_{0.1}$ (a Ni-enriched variant of NMC811). The NCA cathode is likely $Ni_{0.81}Co_{0.14}Al_{0.05}$. A description of the ICP-OES procedure is provided below and the raw data is given in Table SI (available online at stacks.iop.org/JES/167/120532/mmedia).

ICP-OES.—The elemental composition of the NCA and NMC cathodes was determined with an Avio 500 ICP-OES (Perkin Elmer) equipped with a type K1 concentric nebulizer and baffled cyclonic

*Electrochemical Society Member.
[z]E-mail: ypreger@sandia.gov

Table I. Commercial 18650-format lithium-ion battery manufacturer-specified operating bounds.

Battery	LFP	NCA	NMC
Nominal Capacity (Ah)	1.1	3.2	3
Nominal Voltage (V)	3.3	3.6	3.6
Voltage Range (V)	2 to 3.6	2.5 to 4.2	2 to 4.2
Max Discharge Current (A)	30	6	20
Acceptable Temperature (°C)	−30 to 60	0 to 45	−5 to 50
Nominal Mass (g)	39	48.5	47

spray chamber. The instrument parameters were as follows: RF-power 1500 W, 15 L-Ar min^{-1} plasma flow, 0.7 L-Ar min^{-1} nebulizer flow, and 0.2 L-Ar min^{-1} auxiliary gas flow. Prior to analysis, samples of the active material on the Al current collector were digested using a Mars 6 (CEM Corporation) extraction system. Microwave digestion was carried out in two steps, with the first consisting of the addition of sulfuric acid (5 ml) to 0.03–0.05 g of cathode sample in a Teflon microwave vessel. Samples were heated for 0.5 h until they reached a temperature of 260 °C (maximum microwave power, 1800 W) and held at that temperature for 0.25 h. Following cooling and depressurization, hydrochloric acid (3 ml) and nitric acid (3 ml) were added to the Teflon vessel and a second microwave digestion cycle was completed as follows: 0.5 h ramp to 200 °C (maximum microwave power, 1800 W) followed by a hold at that temperature for 10 min. Sample digests were then diluted to 50 ml. These digests were then diluted once more with addition of an yttrium internal standard. Samples were analyzed along with standard elemental reference materials (Inorganic Ventures). The following background-corrected emission lines were chosen for evaluation due to optimal performance: Li (670.784 nm), Ni (231.604 nm), Co (228.616 nm), Mn (257.610 nm), and Al (396.153 nm).

Cycling equipment.—Cycle aging was carried out using an Arbin SCTS and an Arbin high-precision (Model: LBT21084) multi-channel battery testing system. Individual cells were placed into commercially available 18650 battery holders (Memory Protection Devices). The holders were connected to the Arbin with 18 gauge wire and the cable lengths kept below eight feet to minimize voltage drop. During cycling, the cells were placed in SPX Tenney Model T10C-1.5 environmental chambers, which can be controlled between −73 °C and 200 °C. A K- or T-type thermocouple was attached to the skin of each cell under test with Kapton tape to monitor the cell skin temperature.

Cycle aging protocol.—At the start of the study, the as-received cells were placed in thermal chambers for a day to equilibrate to the desired cycling temperatures. Then, the cells were discharged. Each round of cycling consisted of a capacity check, some number of cycles at the designated conditions for that cell, and another capacity check at the end (Scheme 1). The capacity check consisted of three charge/discharge cycles from 0%–100% SOC at 0.5C (a rate of 1C corresponds to the current that will discharge the full capacity of a battery in one hour). 100% SOC is defined as the capacity obtained at a 0.5C constant current charge with a current taper to 0.05 A to the maximum manufacturer-specified charging voltage. The same capacity check protocol was employed for all cells in the study.

A round of cycling for each cell varied from 125 to 1000 cycles, depending on the rate of degradation at the specific test conditions. The cycle count for a round was halved if a cell experienced over 5% capacity loss in the previous round. These adjustments were intended to offer enough granulation in the capacity decline curve to enable observation of any changes in mechanism, while still maintaining a reasonable check-up frequency during a nearly three-year study. Electrochemical impedance spectroscopy (EIS) was completed at intervals of approximately 3% capacity loss, and these results will be expanded upon in a future publication. For the purpose of this publication, the study was considered complete once a cell reached 80% of its initial capacity.

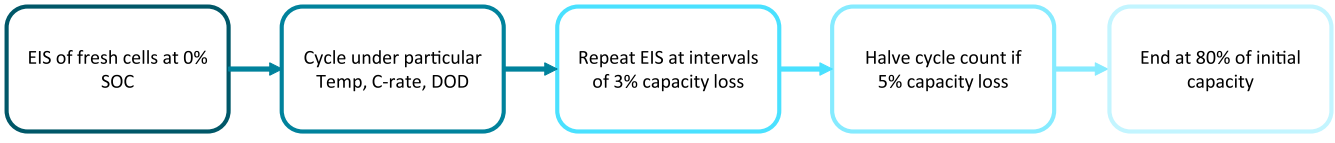
Several abort guidelines were built into the cycling program to avoid potentially abusive conditions for the cells. Cycling was automatically stopped if the cell charge or discharge voltage was more than 0.05 V outside of voltage range limits, and if the cell ever exceeded the manufacturer-specified temperature.

Study conditions.—Table II illustrates the combinations of temperatures, DOD, and discharge currents examined in this study. These values were selected according to a design of experiment approach in order to cover a broad range of manufacturer-recommended parameter space and to identify the general dependence on each variable. To ensure repeatability, each test was performed with at least two cells.

The nominal capacities of the cells were used as references for calculating C-rates. All cells were charged at a rate of 0.5C, per manufacturer guidance. Unlike the other cells, NCA cells were not discharged at 3C since the required current, 9 A, is outside of manufacturer specifications. Cells were cycled at 40%–60% SOC using a constant current (CC) protocol based on capacity limits. Cells were cycled at 20%–80% SOC with a CC protocol using voltage limits established from the discharge capacity curves of fresh cells. Cells cycling at 0%–100% SOC were charged using a constant current constant voltage (CCCV) protocol, with a current taper to 0.05 A. For the 100% DOD regime, LFP cells were cycled from 2 to 3.6 V, NCA cells from 2.5 to 4.2 V, and NMC cells from 2 to 4.2 V. The cycling programs were not adjusted over the course of the study as the cells aged and the SOC labels are based on discharge curves from the fresh cells.

Results and Discussion

General analysis.—The lifetime performance of a battery depends on complex physico-chemical processes influenced by many operating variables. This study considered the influence of three of the variables most readily controlled during operation—temperature, DOD, and discharge rate. In Figs. 1 and 2, the cells are compared based on their capacity retention, discharge energy throughput, and round-trip efficiency (RTE), evaluations that are useful for both laboratory research and field implementation. Figure 1 illustrates the discharge capacity retention vs equivalent full cycle (EFC) count for all cells in the experimental matrix to present an overall picture of cycle-induced aging. In this work, one EFC is based on the nominal capacity of the cell. Therefore, for each cell, the total capacity throughput was divided by the nominal capacity to get the total equivalent full cycle count. The LFP cells exhibit substantially longer cycle life spans under the examined conditions: 2500 to 9000 EFC vs 250 to 1500 EFC for NCA cells and 200 to 2500 EFC for NMC cells. Most of the LFP cells had not reached 80% capacity by the conclusion of this study for the NCA



Scheme 1. Structure of cycle aging study.

Table II. Test matrix for all chemistries[a)].

DOD, Temperature, Discharge Rate[b)]			
40%–60%, 25 °C, 0.5C	0%–100%, 15 °C, 1C	0%–100%, 15 °C, 2C	40%–60%, 25 °C, 3C
20%–80%, 25 °C, 0.5C	0%–100%, 25 °C, 1C	0%–100%, 25 °C, 2C	20%–80%, 25 °C, 3C
0%–100%, 25 °C, 0.5C	0%–100%, 35 °C, 1C	0%–100%, 35 °C, 2C	0%–100%, 25 °C, 3C

a) The cycling conditions noted in the test matrix were applied to LFP and NMC cells. NCA cells were not subjected to any cycling conditions that included a 3C discharge rate, which is outside of the manufacturer-specified current limits for that cell. b) All cells were charged at a rate of 0.5C.

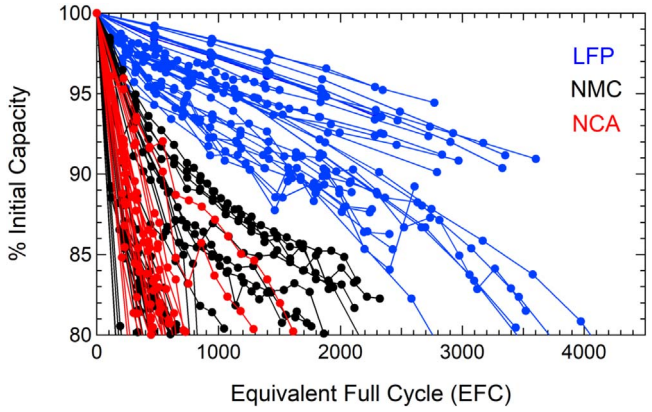


Figure 1. Discharge capacity retention for all LFP (blue), NMC (black), and NCA (red) cells relative to the initial capacity of each individual cell. Circles are data points from the capacity check at the conclusion of each round of cycling and lines are a guide to the eye.

and NMC cells, and their longer-term degradation will be reported in a later work. The spread in the data for each of the chemistries indicates that even within the manufacturer-specified operating bounds there is significant dependence on the specific cycling conditions. Irrespective of the testing conditions, all cells exhibited primarily linear degradation behavior, with slightly more rapid fade at the beginning and end of cycling. This behavior is in agreement with previous models of lithium-ion battery degradation which propose three phases of capacity fade[20,21]:

Phase 1: Sudden drop in capacity as Li is consumed during SEI formation

Phase 2: Linear degradation, generally associated with loss of Li inventory in side reactions

Phase 3: Rapid capacity fade as the cell fails, often attributed to an impedance increase

Figure 2a indicates the EFC for each cell to reach 80% capacity under the given cycling conditions. Though cells may be used beyond 80% capacity in grid applications, this value is a useful benchmark as it is often the reference used by manufacturers in specification sheets to indicate end of life. For LFP cells that have not yet reached 80% capacity, the lifetime was extrapolated based on the present (linear) degradation rate. Among the three chemistries, there is no universal dependence on temperature, DOD, or discharge rate. A more systematic analysis of variable dependence is presented below.

Though EFC is typically the metric by which batteries are compared, cumulative discharge energy may offer more value for field implementation. The EFC may mask degradation differences arising in batteries with different capacity and voltage ranges. Figure 2b indicates the cumulative discharge energy for a cell under each set of cycling conditions at 80% capacity retention. This value was calculated by summing the energy from each individual discharge of the cell. The performance differences between the three chemistries were minimized once the analysis factored in the lower capacity and voltage of the LFP cells (see Table I).

Round-trip efficiency, another important metric for technoeconomic evaluation of LiBs, is shown in Fig. 2c.[22] The RTE for a cycle was calculated by dividing the discharge energy by the charge energy. A single RTE is often assumed for economic evaluations; however, RTE depends substantially on the cycling conditions, including the charge/discharge rate, temperature, SOC, and rest time. The LFP cells show higher RTEs than NCA and NMC cells at all conditions, though the differences are minimized at lower discharge rates. The NCA cells exhibited particular sensitivity to higher discharge rates, with RTEs dropping 5%–10% for an increase in discharge rate from 1C to 2C at all temperatures. The decrease in RTE across all cycling conditions as the cells reach 80% capacity is attributed to the increase in cell resistance as the SEI layer grows.

Capacity fade dependence on cycling variables.— *Temperature dependence.*—Figures 3a–3c show a subset of cycling conditions for each chemistry where only the oven temperature was varied (additional plots in Fig. S1). The capacity fade rate increased with increasing temperature for LFP cells but decreased for NMC cells. The NCA cells did not exhibit a strong temperature dependence in the examined range. Different temperature dependences suggest different dominant degradation mechanisms. Though not observed in this study, the transition between degradation mechanisms within a single cell was previously documented by Waldmann et al.[23] An Arrhenius plot from their work on 18650 NMC/LMO-graphite cells is reproduced in Fig. 4. Below 25 °C, the dominant aging mechanism was Li plating, confirmed by observation of metallic Li. Deposition of Li onto the graphite anode can occur in parallel to intercalation when the anode potential drops below 0 V vs Li/Li^+ (promoted by factors such as increasing SOC, increasing charge rate, and lower temperature).[24] Above 25 °C, the dominant mechanism was SEI (solid-electrolyte interphase) growth, confirmed by post-mortem characterization of SEI thickness on the anodes and correlated to resistance increases in the whole cells. The SEI is formed from the decomposition products of electrolyte solvent and Li salt, a reaction accelerated by increasing temperature.[25] Previous studies of temperature dependence may not have observed the transition between the two degradation mechanisms in the same cell because they did not consider a sufficiently broad temperature range.

The capacity fade data for NMC and LFP cells from the present study was fit in the linear region (after the initial period of rapid capacity fade) to obtain aging rates as a function of temperature. Comparison to the previously reported NMC-LMO data indicates that the tipping point between different mechanisms (the point of minimal degradation in Fig. 4) varies substantially with the chemistry (Table III). For example, previous reports on cycle aging of LFP cells indicate a tipping point at temperatures of 5 °C–10 °C, with degradation rates increasing both above and below this temperature.[26] Studies of LFP cells that considered temperatures only above 20 °C observed the capacity fade increase with increasing temperature (consistent with the present work).[27–29] Studies of NMC cells consistently indicate a tipping point around 35 °C. One report found that minimal capacity fade for NMC cells in cycle aging followed 35 °C > 50 °C > 25 °C[16] and several others found a lower capacity fade rate at 45 °C than 20 °C.[17,30] In contrast to LFP and NMC cells, the NCA cells did not exhibit a strong temperature dependence in the range of 15 °C to 35 °C (Fig. 3c).

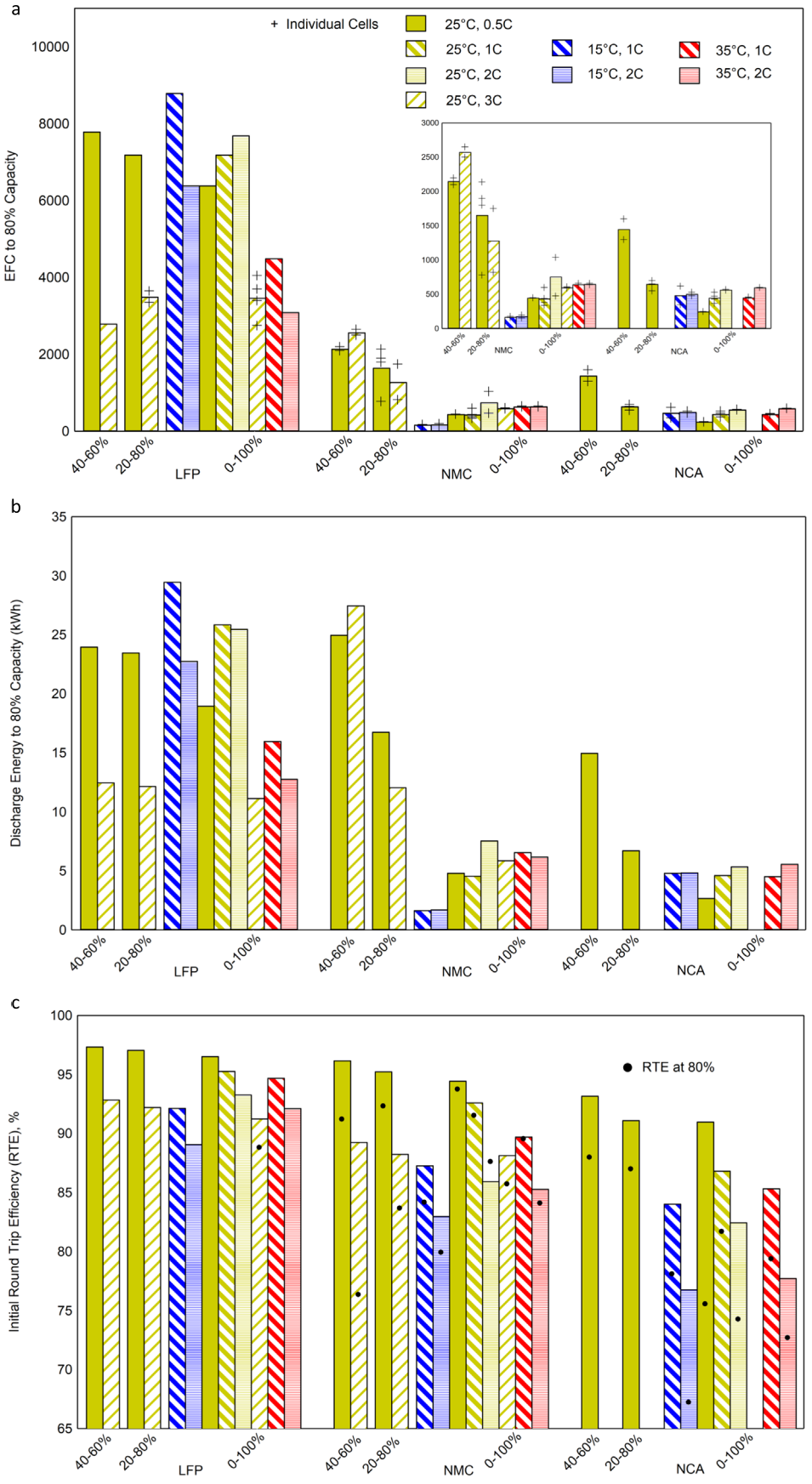


Figure 2. (a) Equivalent full cycle (EFC) count at 80% capacity for all cells and cycling conditions. Each bar represents the average EFC for all cells cycled at that condition. The values for individual cells are noted with a "+". If a bar does not include values for individual cells, then those cells have not yet reached 80% capacity and the indicated EFC is extrapolated based on the present degradation rate for those cells. (b) Cumulative discharge energy at 80% capacity for all cells and cycling conditions. Each bar represents the average discharge energy for all cells cycled at that condition. (c) Round-trip efficiency (RTE) for all cells and cycling conditions. Each bar represents the average initial RTE for all cells cycled at that condition. The RTE at the end of the study is indicated with a dot. If a bar does not include a dot, then those cells have not yet reached 80% capacity.

This behavior is consistent with a previous publication wherein the capacity fade rate of commercial NCA cells increased below 25 °C (due to Li plating) but did not vary significantly between 25 °C and 60 °C.[12] The study did not incorporate materials characterization to explain this lack of temperature dependence, although the authors proposed that the manufacturer had optimized the cell for high

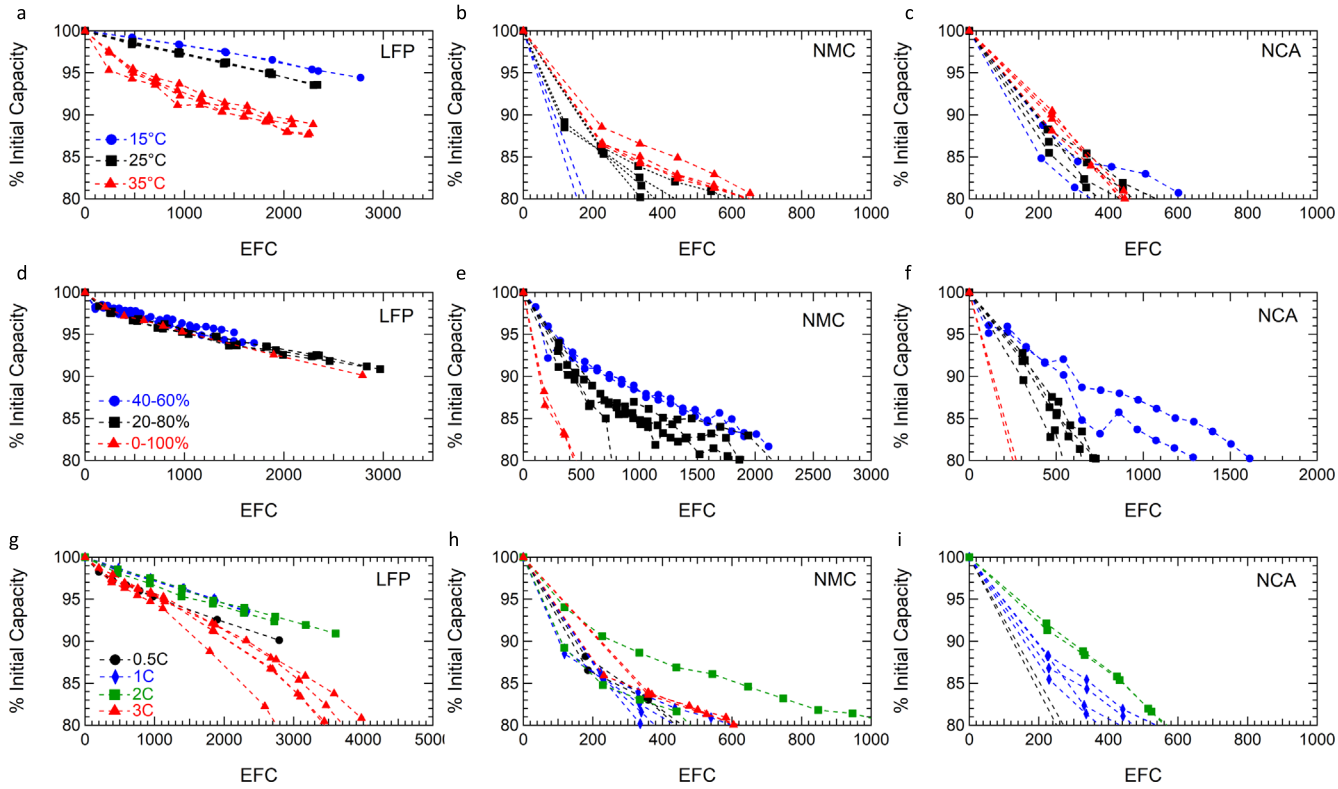


Figure 3. Discharge capacity fade as a function of (a)–(c) temperature, (d)–(f) DOD, and (g)–(i) discharge rate for all chemistries. For each plot, all conditions other than the variable of interest were unchanged. Symbols are data points from the capacity check at the conclusion of each round of cycling and lines are a guide to the eye. (a)–(c) are at 1C discharge and 0%–100% SOC. (d)–(f) are at 0.5C discharge and 25 °C. (g)–(i) are at 0%–100% SOC and 25 °C. Note the different endpoints on the x-axes.

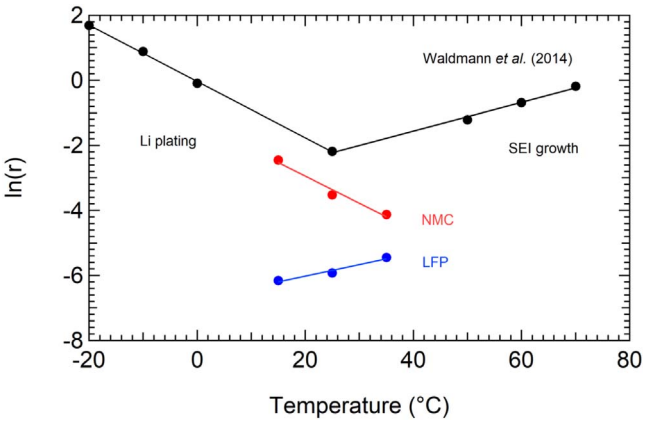


Figure 4. Arrhenius plot for the capacity fade rate of cells. The solid lines correspond to linear fits of the data. Black corresponds to data from Waldmann et al.[23] on 18650 NMC-LMO cells cycled at 1C in a temperature range of −20 °C to 70 °C. Data from the present study for cells cycled at 0%–100% SOC with a 1C discharge rate is shown in red for NMC cells and blue for LFP cells.

temperature operation. A more recent study of comparable NCA cells identified slightly higher degradation at 25 °C than 60 °C.[31]

While the tipping point temperature will certainly be influenced by other cycling conditions, the 30 °C gap in preferred conditions for LFP and NMC cells has implications for best practices in battery thermal management as well as the development of accurate degradation models. Many models assume optimal performance at 25 °C with higher temperatures only accelerating SEI formation. It should be noted that the above analysis only applies to cycle aging studies. For calendar aging studies across LFP,[6,9] NCA,[6] and NMC[6,15] cells, capacity fade consistently decreased with decreasing temperature. Li plating can occur only during charging; thus, SEI growth is the dominant degradation mechanism during calendar aging, with increasing temperatures accelerating the reaction of electrolyte solvent and Li salt.

Depth of discharge dependence.—For all cells in this study, the rate of capacity fade increased with an increasing depth of discharge (Figs. 3d–3f). Greater volume change in the graphite during (de) intercalation increases stress and microcracks.[17,43] Newly-formed cracks enable further reaction between the electrolyte and Li, leading to more SEI formation, loss of Li inventory, and capacity fade. Some studies have shown that only the width of the voltage window matters.[35] In others, the specific placement of the voltage window was significant, a phenomenon variously attributed to:

(1) transition between graphite stages (at specific voltages) with differing lattice parameters enhancing cracking and SEI formation,[15] or
(2) slow Li diffusion at particular voltages leading to Li build-up and graphite particle fracturing[36]

The results of the present study cannot be used to address this discrepancy as the mid-point of the depth of discharge window was not varied.

Compared to LFP[7,33,34] cells, the NCA[35–37] and NMC[15,17,38,39] cells experienced a more dramatic transition in capacity fade from partial to complete DOD and this result is consistent with previous studies. This transition could be attributed to the metal oxide cathodes' higher operating voltages (100% SOC corresponds to 4.2 V for NCA and NMC vs 3.6 V for LFP), which could promote electrolyte oxidation.[44,45] A separate study of LFP cathode half cells charged to different voltages (with an electrolyte of 1 M $LiPF_6$ in EC:DEC 1:1 weight ratio) showed optimal performance at 3.9 V vs Li/Li^+, with no difference in long-term cycling degradation between

Table III. Summary of studies examining temperature, depth of discharge, and discharge rate dependence in commercial cells (cylindrical format, unless otherwise noted).

Chemistry	Reference	Other Conditions[a)]	Performance[b)]
		Temperature (°C)	
	27	0%–100%, 1C/1C	25 > 40 > 50 > 60
	28	0%–100%, 1C/3C	25 > 55
LFP	32[c)]	0%–100%, 1C/1C	5 > −5 > 12 > −20 > 30
	29[c)]	2.2–3.65V, 1C/1C	25 ∼ 35 > 45 > 55 > 65
	this work	*0%–100%, 0.5C/1C*	*15 > 25 > 35*
	12	0%–100%, 0.5C/0.5C	25 ∼ 30 ∼ 40 ∼ 50 ∼ 60 > 20 > 15 > 5 > 0
NCA	31	2.5–4.2 V, 0.64C/0.64C	60 > 25
	this work	*0%–100%, 0.5C/1C*	*15 ∼ 25 ∼ 35*
	23	0%–100%, 1C/1C	25 > 50 > 60 > 70 ∼ 0 > −10 > −20
	16	3.0–4.2 V, 0.5C/1C	35 > 50 > 25
NMC	30	2.75–4.2 V, 1C/1C	45 > 20
	17	various	45 > 20
	this work	*0%–100%, 0.5C/1C*	*35 > 25 > 15*
		Depth of Discharge (% or V)	
	33	60 °C, 0.5C/0.5C	45–55 ∼ 40–60 ∼ 25–75 ∼ 10–90 ∼ 5–95
	34	30 °C, 1C/1C	47.5–52.5 > 20–80 ∼ 0–100 > 45–55 > 35–65 ∼ 25–75
LFP	7	40 °C, 1C/1C	45–55 ∼ 25–75 ∼ 0–100
	this work	*25 °C, 0.5C/1C*	*40–60 > 20–80 ∼ 0–100*
	35	25 °C, 1C/1C	0–60 ∼ 10–70 ∼ 40–100 > 0–100
NCA	36[c,d)]	40 °C, 0.5C/0.5C	3.4–4.0 > 3.0–4.0 > 3.0–4.1 > 3.6–4.2 > 3.4–4.2 > 3.0–4.2 > 3.0–4.3
	37	30 °C, 0.3C/1C	40–60 > 25–75 ∼ 10–90 > 0–100
	this work	*25 °C, 0.5C/1C*	*40–60 > 20–80 > 0–100*
	17	20 °C, 1C/1C	37.5–62.5 > 0–100 > 25–75 > 10–90 > 20–80 ∼ 5–95
	15	35 °C, 1C/1C	47.5–52.5 > 45–55 > 40–60 > 25–75 > 10–90 ∼ 0–100
NMC	38[d)]	25/35/45 °C, 0.33C/1C	40–60 ∼ 32.5–67.5 ∼ 25–75 > 17.5–82.5 > 10–90 > 0–100
	39[d)]	25 °C, 6C/6C	0–20 > 20–40 ∼ 40–60 ∼ 60–80 > 80–100 > 0–100
	this work	*25 °C, 0.5C/1C*	*40–60 > 20–80 > 0–100*
		Discharge Rate (C-rate)	
	40	25 °C, 0%–100%, 0.5C	0.04C > 0.2C ∼ 0.5C > C > 2C
LFP	41[d)]	25 °C, 2.5–3.7 V, 0.5C	0.2C > 1C > 2C > 3C > 4C > 5C
	this work	*15/25/35 °C, 0%–100%, 0.5C*	*0.5C ∼ 1C ∼2C > 3C*
NCA	42	25 °C, 2.5–4.2 V, 0.5C	2C > 1.5C
	this work	*15/25/35 °C, 0%–100%, 0.5C*	*2C > 1C > 0.5C*
	17	0%–100%, 1C	1C > 2C at 20 °C; 1C ∼ 2C at 45 °C
NMC	38[d)]	35 °C, 10%–90%, 0.33C	0.33C ∼ 1C ∼ 2C
	32	22 °C, 2.75–4.2 V, 0.5C	1C > 3C
	this work	*15/25/35 °C, 0%–100%, 0.5C*	*no systematic dependence*

a) Cycling conditions held constant listed in the order of: temperature, depth of discharge given as SOC or voltage range, and charge/discharge rate. b) Better performance corresponds to a lower degradation rate. c) Non-commercial. d) Pouch or prismatic format.

maximum voltages of 3.6 and 4.2 V.[46] These results suggest that the electrochemical cycling behavior of LFP cathodes charged with different upper voltage limits merits further exploration, as the results could vary with the cell manufacturing and electrolyte composition. Irrespective of chemistry, in calendar aging studies, capacity fade consistently increased with SOC, as lower anode potentials enhance electrolyte reduction and Li incorporation into the growing SEI. As in cycle aging studies, NCA and NMC cells exhibited particularly rapid capacity fade at 100% SOC.[6]

Discharge rate dependence.—Higher discharge rates are expected to accelerate capacity fade due to increased stress on the electrodes from rapid volume change.[32,40,41] In Figs. 3g–3h, the discharge rate dependence for NMC and LFP cells appears low. However, for NCA cells, capacity fade decreased with increasing discharge rate (Fig. 3i). Wei et al. observed the same trend and attributed it to increased impedance for cells cycled at lower discharge rates (a physical explanation for this phenomenon was not offered).[42] It is possible that the higher discharge rate may increase cell self-heating (Table SII), leading to improved performance; but, the NCA cells did not exhibit a particularly strong temperature dependence. It is also possible that the shorter period of cycling needed to complete discharge (1 h for 1C vs 0.5 h for 2C) can minimize the degree of calendar aging over the course of hundreds of cycles. Figure S2 shows the capacity fade with respect to time spent cycling rather than EFC and the gap between cells at different discharge rates is slightly reduced. It is unclear why the NCA cells are more strongly influenced by the discharge rate than the other chemistries.

Analysis of variance.—The cycling data was further examined by analysis of variance (ANOVA) to more precisely quantify which conditions contribute to degradation. This also enabled consideration of all cells at once, unlike the variable dependence in previous sections, which only considered systematic variation of single variables. The output variable of interest, % initial capacity, had been measured at different cycle counts across the separate experiments. Therefore, to enable comparison of % capacity at a specific EFC with respect to the factors of interest, regression fits of % capacity vs EFC data were performed for all cells. Occasionally, linear or quadratic fits were used, but in most cases a cubic fit was best. Interpolation was completed only within the range of real data values. General linear models were fit and ANOVA was performed at 200 EFC (before most of the NCA and NMC cells had reached

80% capacity). Three of the four individual factors (cell chemistry, discharge rate, and SOC range) were found to be significant in explaining variability in % capacity. The p values from ANOVA (Table SIII) are below the chosen significance level of 0.05. Additionally, there was a significant interaction between cell chemistry and SOC range, and cell chemistry and temperature. Residual plots (Fig. S3) from this model fit show that the assumptions of randomness, constant variance, and normally distributed residuals are all reasonable. In addition, no concerning patterns are seen.

Figure 5 shows the main effects and interactions plot for all four factors at 200 EFC, demonstrating the importance of not drawing general conclusions about variable dependence for different chemistries. Across all of the tested cells, the % capacity does not change systematically across discharge rate and temperature (Figs. 5b, 5d). Cell chemistry and SOC range have larger effects across their respective levels (Figs. 5a, 5c). For example, at the same EFC, LFP cells have retained on average 7% more capacity than NCA cells and 9% more capacity than NMC cells. Several factors are involved in significant interactions with each other. Figure 5f shows that the SOC range affects % capacity for the NCA and NMC cells similarly (5%–10% lower at 0%–100%), but SOC range has little effect on the capacity for LFP cells. Additionally, temperature affects % capacity for NMC and LFP cells in opposing trends (Fig. 5g). The NMC cells likely exhibit a less systematic trend between 15 and 35 °C because this analysis factors in all of the cells at 25 °C cycled at intermediate SOCs, while Figs. 3b and 4 focused exclusively on the influence of temperature.

Consistency of literature cycling data.—Battery degradation models and conclusions about the performance of particular chemistries are often based on a single data set. To probe the validity of this approach, the degradation of the cells in this study was compared to that of similar commercial 18650 cells examined in previous studies. Figure 6 shows a subset of these comparisons and the rest are given in Fig. S4. Degradation data for cells from the same manufacturer appears consistent across publications, even those separated by several years (Figs. 6b, 6c). However, for cells from different manufacturers sometimes the degradation rate is the same (Fig. 6e) and sometimes it is not (over three times difference in cycle count to 80% capacity in Fig. 6f). These differences suggest that lifetime prognostics based on a particular cell from a particular manufacturer cannot be broadly extrapolated, even to other cells with the same standard form factor, chemistry, and capacity. Subtle variations in materials, such as electrolyte composition, can substantially impact battery lifetime (though that level of detail would not be available on a basic battery specification sheet). Empirical battery degradation models would benefit from the incorporation of larger data sets and reporting values with a standard deviation to give users a better sense of the true lifetime of these cells. However, the analysis above, particularly the comparison in Table III, shows that even though precise lifetimes may differ, variable dependence trends are broadly consistent within a particular chemistry.

Conclusions

Commercial Li-ion batteries based on NMC, NCA, and LFP chemistries were cycled with varying temperature, depth of discharge, and discharge rate. The capacity and discharge energy retention, as well as the round-trip efficiency, were compared. The dependence on each cycling variable was analyzed qualitatively as well as by analysis of variance. Key insights from this work include:

(1) Even within manufacturer specified operating ranges, the equivalent full cycle count at 80% capacity varied up to thousands of cycles depending on the conditions.
(2) LFP cells had the highest cycle lifetime across all conditions, but this performance gap was reduced when cells were compared according to the discharge energy throughput. The latter metric factored in the lower capacity and lower voltage of the LFP cells, illustrating the importance of identifying the appropriate metrics for each application.
(3) The RTE can vary up to 10% among fresh cells depending on the cycling conditions and can decrease over 5% as a cell ages. LFP cells generally had higher RTEs at all conditions and for all cells, RTE consistently decreased with increasing discharge rate.
(4) Based on the current work and a review of previous commercial cell studies, trends in temperature, depth of discharge, and discharge rate dependence are chemistry specific. Variable dependence in one chemistry should not be broadly extrapolated to all lithium-ion batteries.
(5) In the 15 °C to 35 °C temperature range, the capacity fade rate increased with increasing temperature for LFP cells but decreased for NMC cells, indicating different dominant degradation mechanisms. These results illustrate the value of varying multiple temperatures within a normal operating range rather than looking solely at extreme temperatures. The gap in preferred conditions for LFP and NMC cells has implications for battery thermal management. A survey of the literature and

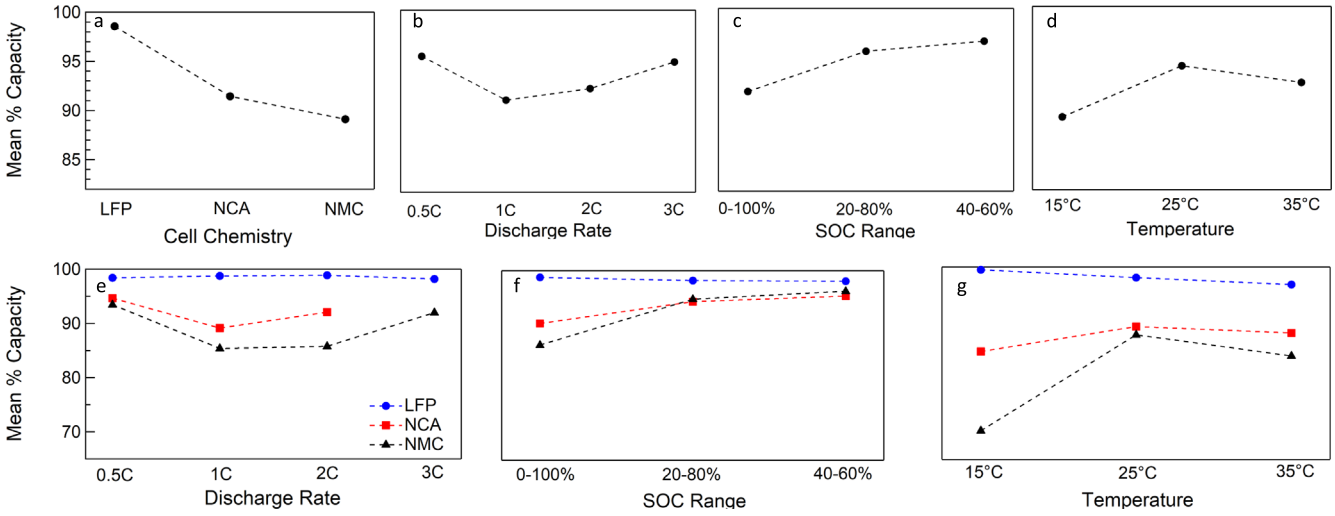


Figure 5. Main effects (a)–(d) and interactions (e)–(g) plots for model fit at 200 EFC. Mean % capacity refers to the average value for all cells at the specified conditions at 200 EFC. This value is derived from regression fits of the % initial capacity vs EFC data shown earlier since the % initial capacity of all cells had been measured at slightly different cycle counts across the separate experiments.

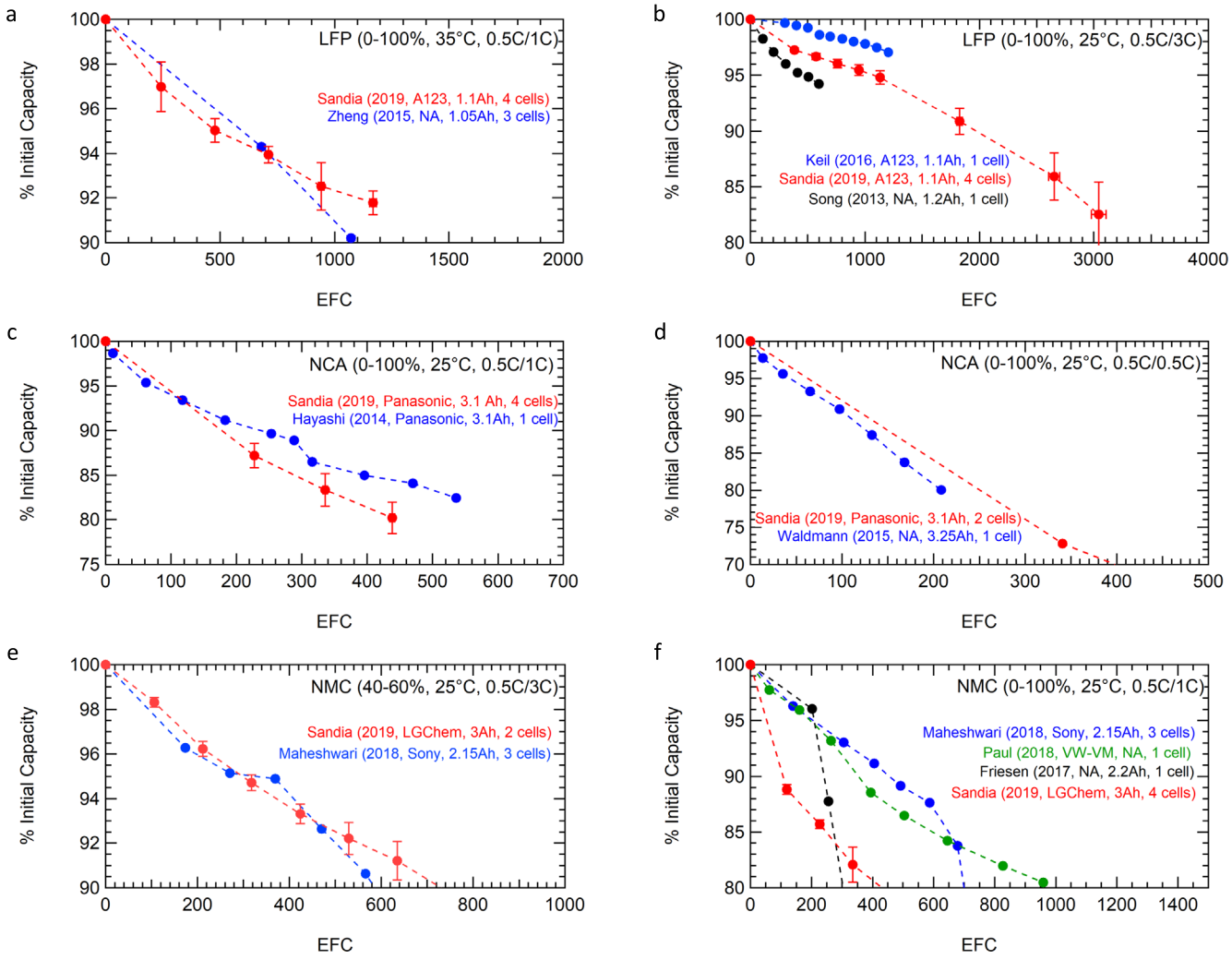


Figure 6. Comparison of battery cycling capacity fade across studies. The chemistry and cycling conditions, given as DOD, temperature, and charge/discharge rate, are noted for each plot. For each data set, the year of publication, cell manufacturer, cell capacity, and number of cells cycled under the specified conditions are noted (when provided in the original publication). "NA" indicates that the specified information was not available. The lines are a guide to the eye and error bars are based on standard deviation when data for multiple cells was available. All references to previous studies were presented in Table III except for Hayashi et al. 2014[47] in (c) and Paul et al. 2018[48] in (f).

the results here suggest that LFP cells are more suited for lower temperature applications.

(6) The NMC and NCA cells exhibited a stronger dependence on depth of discharge, with greater sensitivity to full SOC range cycling than LFP cells.

(7) Battery degradation models would benefit from the incorporation of larger data sets and reporting values with a standard deviation. Most models are evaluated against a single experimental data set, but a comparison of the degradation data in this study to previous commercial cell cycling studies shows the variation possible even under the same conditions.

Future work will include combining electrochemical and materials characterization to identify the origin of the varying lifetimes observed in this study. A subset of the cells will be cycled beyond 80% capacity to identify the causes and early warning signs of transition from linear degradation to rapid capacity fade.

One of the primary difficulties in completing this analysis lay in comparing the data to previous published results, which were typically reported as plots rather than raw data. Thus, batteryarchive.org was created as a searchable repository for easy visualization, analysis, and comparison of battery data across institutions. All cycling files from the present study have been uploaded to this site and we are currently working with other groups with large data sets to share them here. This aggregation of data sets is intended to facilitate future experimental and modeling efforts.

Acknowledgments

This work was supported by the US Department of Energy Office of Electricity, Energy Storage Program. The authors wish to thank Dr. Imre Gyuk for his support of research advancing safety and reliability in stationary energy storage. We would like to thank Dr. Valerio de Angelis for his substantial efforts in developing batteryarchive.org and the CUNY Energy Institute, part of the City College of New York, for providing site access. We are also grateful to Drs. Daniel Wesolowski, Reed Wittman, and Loraine Torres-Castro for thoughtful feedback on the manuscript. Sandia National Laboratories is a multi-mission laboratory managed and operated by National Technology and Engineering Solutions of Sandia, LLC., a wholly owned subsidiary of Honeywell International, Inc., for the U.S. Department of Energy's National Nuclear Security Administration under contract DE-NA-0003525. This paper describes objective technical results and analysis. Any subjective views or opinions that might be expressed in the paper do not necessarily represent the views of the U.S. Department of Energy or the United States Government.

Author contributions

H.M.B. and S.R.F. designed the original study. A.F. and Y.P. executed the cycling experiments, and J. R.-K. and B.W. Juba completed ICP. Y.P. carried out the general data analysis and wrote the paper, with D.L.C. contributing to the statistical analysis. All authors participated in discussion of the results, as well as the preparation of the paper.

ORCID

Yuliya Preger https://orcid.org/0000-0001-8558-2529
Jessica Romàn-Kustas https://orcid.org/0000-0003-1879-0234
Babu Chalamala https://orcid.org/0000-0003-0469-636X

References

1. B. Diouf and R. Pode, *Renew. Energy*, **76**, 375 (2015).
2. T. M. Gür, *Energy Environ. Sci.*, **11**, 2696 (2018).
3. DOE Global Energy Storage Database, https://sandia.gov/ess-ssl/global-energy-storage-database/ (accessed on 16th August 2020).
4. M. Dubarry and B. Y. Liaw, *J. Power Sources*, **194**, 541 (2009).
5. M. Kassem, J. Bernard, R. Revel, S. Pélissier, F. Duclaud, and C. Delacourt, *J. Power Sources*, **208**, 296 (2012).
6. P. Keil, S. F. Schuster, J. Wilhelm, J. Travi, A. Hauser, R. C. Karl, and A. Jossen, *J. Electrochem. Soc.*, **163**, A1872 (2016).
7. M. Lewerenz, J. Münnix, J. Schmalstieg, S. Käbitz, M. Knips, and D. U. Sauer, *J. Power Sources*, **345**, 254 (2017).
8. S. Sun, T. Guan, P. Zuo, Y. Gao, X. Cheng, C. Du, and G. Yin, *ChemElectroChem*, **5**, 2301 (2018).
9. M. Naumann, M. Schimpe, P. Keil, H. C. Hesse, and A. Jossen, *J. Energy Storage*, **17**, 153 (2018).
10. A. J. Crawford, Q. Huang, M. C. W. Kintner-Meyer, J.-G. Zhang, D. M. Reed, V. L. Sprenkle, V. V. Viswanathan, and D. Choi, *J. Power Sources*, **380**, 185 (2018).
11. K. A. Severson et al., *Nat. Energy*, **4**, 383 (2019).
12. T. Waldmann, M. Kasper, and M. Wohlfahrt-Mehrens, *Electrochim. Acta*, **178**, 525 (2015).
13. P. Keil and A. Jossen, *J. Electrochem. Soc.*, **164**, A6066 (2017).
14. M. Dubarry, A. Devie, and K. McKenzie, *J. Power Sources*, **358**, 39 (2017).
15. M. Ecker, N. Nieto, S. Käbitz, J. Schmalstieg, H. Blanke, A. Warnecke, and D. U. Sauer, *J. Power Sources*, **248**, 839 (2014).
16. S. F. Schuster, T. Bach, E. Fleder, J. Müller, M. Brand, G. Sextl, and A. Jossen, *J. Energy Storage*, **1**, 44 (2015).
17. A. Maheshwari, M. Heck, and M. Santarelli, *Electrochim. Acta*, **273**, 335 (2018).
18. H. M. Barkholtz, A. Fresquez, B. R. Chalamala, and S. R. Ferreira, *J. Electrochem. Soc.*, **164**, A2697 (2017).
19. H. M. Barkholtz, Y. Preger, S. Ivanov, J. Langendorf, L. Torres-Castro, J. Lamb, B. Chalamala, and S. R. Ferreira, *J. Power Sources*, **435**, 226777 (2019).
20. R. Spotnitz, *J. Power Sources*, **113**, 72 (2003).
21. X.-G. Yang, Y. Leng, G. Zhang, S. Ge, and C.-Y. Wang, *J. Power Sources*, **360**, 28 (2017).
22. K. Mongird, V. Viswanathan, P. Balducci, J. Alam, V. Fotedar, V. Koritarov, and B. Hadjerioua, Energy Storage Technology and Cost Characterization Report, Pacific Northwest National Laboratory (2019), https://doi.org/10.2172/1573487.
23. T. Waldmann, M. Wilka, M. Kasper, M. Fleischhammer, and M. Wohlfahrt-Mehrens, *J. Power Sources*, **262**, 129 (2014).
24. T. Waldmann, B.-I. Hogg, and M. Wohlfahrt-Mehrens, *J. Power Sources*, **384**, 107 (2018).
25. S. J. An, J. Li, C. Daniel, D. Mohanty, S. Nagpure, and D. L. Wood III, *Carbon*, **105**, 52 (2016).
26. V. Ruiz, A. Kriston, I. Adanouj, M. Destro, D. Fontana, and A. Pfrang, *Electrochim. Acta*, **240**, 495 (2017).
27. L. Tan, L. Zhang, Q. Sun, M. Shen, Q. Qu, and H. Zheng, *Electrochim. Acta*, **111**, 802 (2013).
28. H. Song, Z. Cao, X. Chen, H. Lu, M. Jia, Z. Zhang, Y. Lai, J. Li, and Y. Liu, *J. Solid State Electrochem.*, **17**, 599 (2013).
29. S. Yi, B. Wang, Z. Chen, R. Wang, and D. Wang, *Ionics*, **25**, 2139 (2019).
30. A. Friesen, X. Mönnighoff, M. Börner, J. Haetge, F. M. Schappacher, and M. Winter, *J. Power Sources*, **342**, 88 (2017).
31. H. Wang, S. Frisco, E. Gottlieb, R. Yuan, and J. F. Whitacre, *J. Power Sources*, **426**, 67 (2019).
32. T. S. Bryden, A. Holland, G. Hilton, B. Dimitrov, C. Ponce de León Albarrán, and A. Cruden, *Energy Procedia*, **151**, 194 (2018).
33. J. Wang, P. Liu, J. Hicks-Garner, E. Sherman, S. Soukiazian, M. Verbrugge, H. Tataria, J. Musser, and P. Finamore, *J. Power Sources*, **196**, 3942 (2011).
34. E. Sarasketa-Zabala, I. Gandiaga, E. Martinez-Laserna, L. M. Rodriguez-Martinez, and I. Villarreal, *J. Power Sources*, **275**, 573 (2015).
35. S. Watanabe, M. Kinoshita, T. Hosokawa, K. Morigaki, and K. Nakura, *J. Power Sources*, **260**, 50 (2014).
36. J. Li, J. Harlow, N. Stakheiko, N. Zhang, J. Paulsen, and J. Dahn, *J. Electrochem. Soc.*, **165**, A2682 (2018).
37. Y. Zhang, R. Xiong, H. He, X. Qu, and M. Pecht, *Appl. Energy*, **255**, 113818 (2019).
38. J. de Hoog, J.-M. Timmermans, D. Ioan-Stroe, M. Swierczynski, J. Jaguemont, S. Goutam, N. Omar, J. Van Mierlo, and P. Van Den Bossche, *Appl. Energy*, **200**, 47 (2017).
39. Y. Gao, J. Jiang, C. Zhang, W. Zhang, and Y. Jiang, *J. Power Sources*, **400**, 641 (2018).
40. M. Dubarry, C. Truchot, and B. Y. Liaw, *J. Power Sources*, **258**, 408 (2014).
41. S. Sun, T. Guan, X. Cheng, P. Zuo, Y. Gao, C. Du, and G. Yin, *RSC Adv.*, **8**, 25695 (2018).
42. D. Cui, J. Wang, A. Sun, H. Song, and W. Wei, *Scanning*, 2593780 (2018), https://www.hindawi.com/journals/scanning/2018/2593780/.
43. H. Zheng, L. Tan, L. Zhang, Q. Qu, Z. Wan, Y. Wang, M. Shen, and H. Zheng, *Electrochim. Acta*, **173**, 323 (2015).
44. A. S. Mussa, M. Klett, M. Behm, G. Lindbergh, and R. W. Lindström, *J. Energy Storage*, **13**, 325 (2017).
45. B. Lunz, Z. Yan, J. B. Gerschler, and D. U. Sauer, *Energy Policy*, **46**, 511 (2012).
46. H. Zheng, L. Chai, X. Song, and V. Battaglia, *Electrochim. Acta*, **62**, 256 (2012).
47. T. Hayashi, J. Okada, E. Toda, R. Kuzuo, N. Oshimura, N. Kuwata, and J. Kawamura, *J. Electrochem. Soc.*, **161**, A1007 (2014).
48. N. Paul, J. Keil, F. M. Kindermann, S. Schebesta, O. Dolotko, M. J. Mühlbauer, L. Kraft, S. V. Erhard, A. Jossen, and R. Gilles, *J. Energy Storage*, **17**, 383 (2018).